



## Physicochemical Impacts of Formation and Assembly of Quantum Dots Flowery Island of the (Sr-Cr-O) Semiconductor

Basma A. A. Balboul<sup>\*ab</sup>, Moustafa Shaban A. Selim<sup>b</sup>

<sup>a</sup> Department of Chemistry, college of Science, Jouf University, P.O. Box 2014, Aljouf, Saudi Arabia

<sup>b</sup> Department of Chemistry, Faculty of Science, Minia University 61519, El-Minia, Egypt



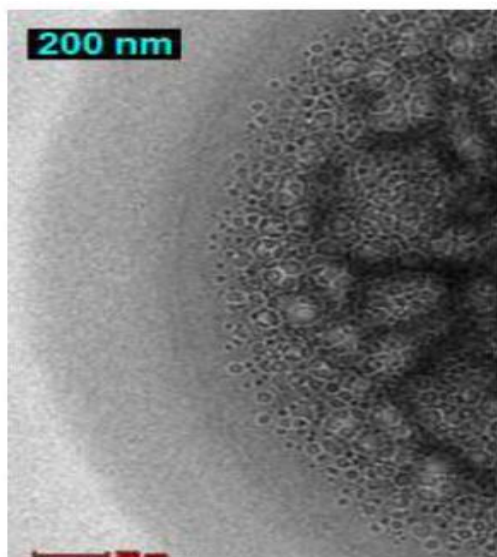
CrossMark

### Abstract

In this paper, we fabricate a reactive self-assembled nanostructure of strontium chromium oxygen system (Sr-Cr-O). The ternary oxide SrCrO<sub>4</sub> has been prepared as a QDs decorated superlattice. Course of formation as well as the obtained composition was analyzed by a combination of Thermogravimetry (TGA), X-ray diffraction (XRD), UV-vis diffuse reflectance spectra (DRS), scanning electron microscopy in association with EDX and high resolution transmission electron microscopy (TEM). The obtained nanostructure was determined to be composed of SrCrO<sub>4</sub> as the major phase and SrCrO<sub>3</sub>/ SrO<sub>1.95</sub> as the minor phases. Excitonic absorption signatures in optical spectroscopy confirmed that quantum confinement is preserved. The methodology involves a modified co-precipitation method. Moreover, excellent UV-visible-light photocatalytic performance was improved toward Methylene blue dye.

**Keywords:** SrCrO<sub>4</sub>, QDs, self-assembly, Nanoparticles, Thermal analysis.

### Graphical abstract



### Highlights

Reactive self-assembled nanostructured of the strontium chromium oxygen system (Sr-Cr-O).  
Efficient Photocatalytic degradation rate of MB dye

### 1. Introduction

Nanostructured oxide semiconductor materials have attracted great interest in recent years because of the unusual mechanical, electrical and optical properties and because of the combination of bulk and surface properties to the overall behavior [1,2]. The semiconductor quantum dots (QDs), have attracted many interests, their small size and their high surface to volume ratio and quantum confinement of exciton, affect their optical and electronic properties and make them different from the same larger particles [3,4]. Colloidal techniques enable the synthesis and manipulation of semiconductor materials with different structures [5]. These structures may be prepared by varying the reaction conditions, surfactants or both.

Sr-Cr-O system has been widely studied as interesting materials (SrCrO<sub>4</sub> and SrCrO<sub>3.8</sub>) with functional properties [6,7] and potential applications including photosensitization, photoluminescence, scintillation [8] catalysis [9] and as yellow pigment [10, 11]. Despite the several promising applications of SrCrO<sub>4</sub> due to its high thermal stability, crystallinity, etc., The use of SrCrO<sub>4</sub> together with

\*Corresponding author e-mail: [babalboul@ju.edu.sa](mailto:babalboul@ju.edu.sa); [basma.balboul@mu.edu.sa](mailto:basma.balboul@mu.edu.sa)

Receive Date: 05 March 2021, Revise Date: 26 March 2021, Accept Date: 28 March 2021

DOI: 10.21608/EJCHEM.2021.65404.3424

©2021 National Information and Documentation Center (NIDOC)

TiO<sub>2</sub> was also explored as a photocatalyst for the photodegradation of Rhodamine B and rhodamine 6G [8, 12]. Recently, R. Khobragade et al [9] reported that Strontium chromate catalyst is stable and shows significantly improved intrinsic catalytic performance for (Pt) group metal (PGM) based catalyst for diesel (PM) (Particulate Matter) oxidation. Moreover SrCrO<sub>4</sub> has been synthesized as nanostructures including nanospheres, nanorods, dumbbells and long nanowires by different synthetic routes [13- 15].

There are two primary goals of this study: 1- the first goal is to prepare a modified nano- mixed metal oxide semiconductor of the (Sr-Cr-O) system 2- the second goal is to characterize and highlight the efficient properties of the prepared material. In this research paper, we have successfully prepared a self-assembled nanostructured of Strontium chromium oxide system composed of SrCrO<sub>4</sub> as a major phase and SrO<sub>1.95</sub>/SrCrO<sub>3</sub> as minor crystals with different morphologies.

## 2. Experimental:

### 2.1. Materials:

Chromium nitrate nonahydrate Cr (NO<sub>3</sub>)<sub>3</sub>.9H<sub>2</sub>O (purity 99%) was obtained from BDH laboratory reagents, England. Strontium nitrate (purity 98 %) and it was used as provided by LOBA Chemie. Methylene blue was obtained from Merck. Hydrochloric acid and Ammonia solution (33% product of El-Nasr Company, Egypt). Citric acid from ADWIC Company.

Synthesis of Sr-Cr-O semiconductors :

The self-assembled structure was simply prepared by calcination of the reaction mixture at 800°C for 4 hours containing specific amounts of chromic nitrate nonahydrate, strontium nitrate and citric acid. Chromium nitrate [Cr(NO<sub>3</sub>)<sub>3</sub>.9H<sub>2</sub>O] and strontium nitrate [Sr(NO<sub>3</sub>)<sub>2</sub>] as precursors were dissolved together in a 1 L flask with 250 ml deionized water in 1 : 1.5 molar ratio. A specified amount of citric acid (C<sub>6</sub>H<sub>8</sub>O<sub>7</sub>) was added to the solution as a surfactant and coating material. Dilute ammonia solution was added drop wise with constant stirring until the precipitation was completed (at pH = 9). The supernatant liquid was decanted and the obtained product was then washed with deionized water, the residue was dried for 24 h at 100° C in an oven and the obtained powder was heated in a porcelain crucible up to 800° C for 4 hours. Experimental techniques used in the characterization of (Sr-Cr-O) semiconductor are described in the next section and the sample was denoted in the text as (SCO). The

same experimental procedures were repeated to prepare the sample using different amount of citric acid, to explore the effect of surfactant % on the morphology of the studied system. The latter prepared sample was denoted in the text as (SCO)\*.

### 2.2. Methods of Characterization of (Sr-Cr-O) semiconductor:

The thermal studies of the oven dried precursor powder was characterized by TGA/DTA by shimadzu analyzer (Japan), when heating a small amount of 5 mg up to 800° C with a heating rate of 10 dpm under an air atmosphere.

The structural features of the as prepared sample were characterized by X-ray powder Diffraction (XRD). The XRD pattern was accomplished through methods of a model JSX-60 PA Jeol diffractometer (Japan) equipped with Ni-filtered CuK $\alpha$  radiation ( $\lambda = 0.15416$  nm). In view of scans in the range  $4^\circ \leq 2\theta \leq 80^\circ$ , the  $2\theta$  and relative intensity ( $I/I^\circ$ ) values acquired of the observed diffraction peaks matched with the ones filed in the JCPDS database for phase identification purposes [16] (International Center for Diffraction Data). Moreover, the elemental composition of the (SCO) samples can be examined by the EDX line profiles of the samples. EDX analyses were performed on a model QUANTA FEG 250.

The morphology of the particles as well as the actual composition of the Sr-Cr-O oxides were obtained by scanning electron microscopy (SEM) (Joel SEM 5004 LV) and transmission electron microscope (TEM: Techni G2 Sprit Twin). The HRTEM analysis is used to know the particle size of (Sr-Cr-O) system.

FTIR spectra were measured using a model 410 Jasco FT-IR spectrophotometer (Japan). The measurement was at 4000-400 cm<sup>-1</sup> with the resolution of 4 cm<sup>-1</sup>, the spectra were taken of lightly loaded (<1%) thin discs of KBr-supported test materials.

Electrical conductivity measurements for the semiconductor samples were performed at room temperature. The test samples were lose powder pressed at room temperature with the help of a hydraulic pressure instrument at 25 kN pressure for 10 min. Measurements were performed on pressed pellets by using a 4-in-lineprobe dc electrical conductivity-measuring technique Scientific Equipment, The average thickness of the sample pellets was accurately measured about 0.6 mm.

UV- Vis analysis was carried out using Thermo Electron – Visionpro Software V4.10. UV–vis DRS spectra of the samples were measured using a UV-3600 plus spectrometer (Shimadzu, Japan). The spectra were collected at 200–900 nm using BaSO<sub>4</sub> as a reflectance reference.

Photocatalytic Degradation of Dye=

$$C_0 - C / C_0 \times 100 \quad (\text{eq. 1})$$

Methylene blue (MB) was used as an exemplary of organic pollutants to assess the photocatalyst. The photocatalytic activity of the sample was performed by comparing the degradation of Methylene blue (50 mL aqueous solution containing 3 mg/L MB) containing 30 mg of the as-prepared catalyst under light irradiation excited from 400W mercury lamp. The pH value of dye solution was adjusted to the natural value pH 6.5 by 1M HCl while the radiation distance between the lamp and sample was 10 cm. Before illumination, the suspension was sufficiently stirred in a dark environment for 45 min to achieve adsorption-desorption equilibrium between the catalysts and the dye, the zero measurement was taken, and then the solution was irradiated while stirring. Five milliliters from the solution was taken at regular intervals to monitor the absorbance change using UV-Vis spectrophotometer (Shimadzu UV 2550) at 663 nm. The samples taken were centrifuged at 5000 rpm for 30 min to remove the catalyst before measuring the absorbance. The degradation efficiency was determined according to the following equation

$$\text{The degradation efficiency (\%)} = C_0 - C / C_0 \times 100$$

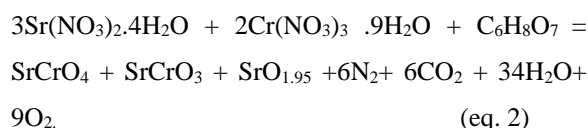
### 3. Results and discussion

#### 3.1. Course of formation

Ternary nanocrystals are an important class of semiconductors whose properties can be adjusted by changing the nanocrystal size as well as composition. The synthesis of ternary nanocrystals represents a challenging task due to the presence of two metal salts in the reaction mixture (the oven dried precursor powder).

The TG curve (Fig.1a) is shown to display two stages, the first mass loss stage at low temperature

(commences 48° ends 229°C) with its DTA endothermic peak centered at 87°C was supposed to be the dehydration of the coordinated water in the formed complex of dried mixture as well as the primary oxidation of citric acid (CA). According to many researchers [17], CA appears to be an excellent fuel for synthesis of pure oxide powders with high surface area. Apparently, The second stage of reaction is faster, involves strongly overlapped, exothermic thermal events which occur over the temperature range from 400 to 460°C. The mentioned events and characteristics are set out in (table 1). (400 to 460°C). In The second stage a combustion (glowing) reaction was initiated and proceeded with the diffusion of oxygen from the ambient atmosphere to form the expected oxides. The rapid liberation of large volumes of volatiles from reactant mixtures prevent agglomeration of particles and result in the production of nanoparticles of fluffy form. Indeed, the combustion of reactive materials in higher temperature regime 400-460, (Fig.1b), improves the crystallinity of the material and decreases the amount of harmful gases (NO<sub>x</sub>) which is due to in situ reduction by fuel fragments (CA) such as CH<sub>4</sub> that is formed during the decomposition of citric acid [10]. Thus the proper selection of the fuel type reduce or prevent the formation of hazardous gases and yields nitrogen, water and carbon dioxide, thereby, providing an environment-friendly fabrication process. The overall reaction may be described as follows



From 500-800°C, the DTA curve shows no further thermal peaks, revealed a good thermal stability of the nano-oxide. Clearly, the reaction pathway is different than that reported by baharat et al [8] due to the modified methodology as well as the adjustment of reaction stoichiometry.

Table 1: TG/ DTA Characteristics of thermal events encountered throughout the (SCO) decomposition course (at 20 °C/min) in air.

Stages	Thermal events	Temperature range/°C	Mass loss %	T <sub>max</sub> /°C	ΔT/T
First stage	I	45.0-230	-12.57%	87.7	Endothermic
Second Stage	II	332-470	-64%	340	Exothermic
	III			402	Exothermic
	IV			406	Exothermic
	V			410	Exothermic
	VI			413	Exothermic

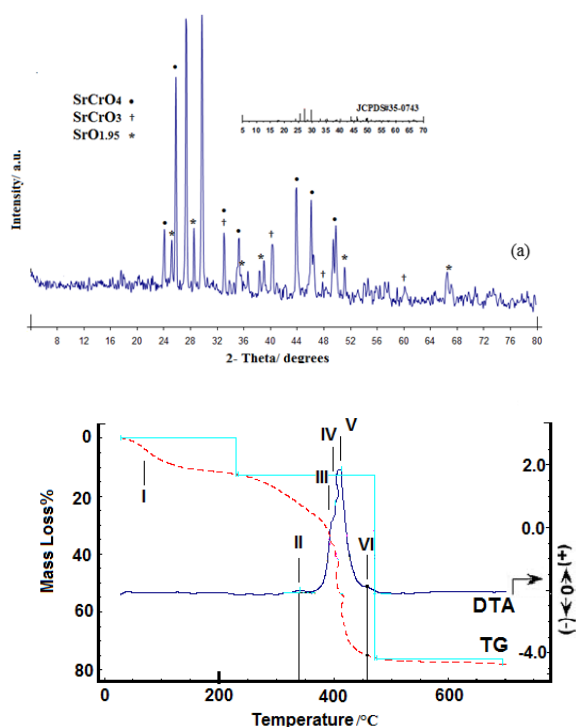


Fig.1: (a) TG and DTA curves obtained (at 10°C/min) for the precursor powder in a dynamic atmosphere of air (50 cm<sup>3</sup>/min). The Roman numerals (I–VI) indicate locations where the thermal events encountered are maximized, as further cited in Table 1, (b) XRD Patterns of (SCO) self-assembled phases heat treated at 800° for 4h.

### 3.2. Structural characteristics:

Many researchers have been studied extensively the self-assembled nanostructured semiconductors to realize the effect of crystal structure, crystallinity, and particle size on the tunability of specific electronic and photonic properties. The XRD pattern of the sample heat treated at 800 °C for 4 h (Fig. 1b), gives evidence of the growth of monoclinic SrCrO<sub>4</sub>, cubic perovskite SrCrO<sub>3</sub> and tetragonal SrO<sub>1.95</sub> QDs in the matrix. For SrCrO<sub>4</sub> NPs, the peak positions ( $2\theta = 25.8, 27.6, 29.7, 43.8, 46.1, 49.4, 66.4$ ) match with JCPDS card no. 35-0743 file. The lower intensity diffraction peaks at ( $2\theta = 24.1, 33, 40.2, 47.8$ ) and ( $2\theta = 25.2, 28.5, 30.1, 35.2, 46.3, 49.8, 51.1, 66.7$ ), matching well with JCPDS card no. 20-1192 and JCPDS card no. 82-0915 for SrCrO<sub>3</sub> and SrO<sub>1.95</sub>, respectively. The average crystallite size of the Sr-Cr-O system was determined via origin pro software applying XRD data using the well-known Scherrer's formula

$$D = k \lambda / \beta \cos \theta$$

where  $k$  is a constant (0.89),  $\lambda$  the XRD wavelength corresponds to 1.54 nm of the copper

source and the energy of the electron beam is 8.04 KeV,  $\beta$  the corrected half-width of the strongest diffraction peak and  $\theta$  the diffraction angle [18]. Accordingly the crystallite sizes of the three phases present in the sample are determined to be in accordance with TEM results but slightly larger in size: The calculated crystallite size of the major phase SrCrO<sub>4</sub> is equal to 5.3 nm, SrCrO<sub>3- $\delta$</sub>  is equal to be 1.2 nm and that of the minor phase is equal to 0.45 nm which appears slightly larger than the real particle size calculated by TEM.

In support to the XRD analysis, FTIR spectrum of the sample (SCO) calcined at 800 °C (Fig. 2) clearly indicated the various vibrations of the as-prepared NPs. Sr-Cr-O system was expected to exhibit absorptions over the range 1000-400 cm<sup>-1</sup> [8]. The internal modes usually exhibited by CrO<sub>4-2</sub> are symmetric, asymmetric stretching modes as well as symmetric and asymmetric bending modes. The reported FTIR data for SrCrO<sub>4</sub> phase were at 924, 902, 884, and 869 cm<sup>-1</sup> correspond to Cr-O asymmetric stretching mode [8, 19- 21]. The O-Cr-O asymmetric bending mode usually found below 450 cm<sup>-1</sup>. The spectrum (Fig. 2) exhibits the same band structure reported for CrO<sub>4-2</sub> in addition to another repeated band structure having nearly the same absorptions, slightly shifted to higher frequencies. These characteristic peaks (in our experiment) appear at 937, 926, 924, 915, 904, 902, 884, 869 cm<sup>-1</sup>. The smaller intensity sharp bands appear at lower frequencies (426 and 406 cm<sup>-1</sup>) resulted from the symmetric and asymmetric bending modes of vibrations of the O-M-O bands. The stretching and flexion mode of the Sr- O is below the 150 cm<sup>-1</sup> which is past the recorded range. The broad bands observed at 3420 and 3343 cm<sup>-1</sup> correspond to stretching vibrations of the surface hydroxyls and absorbed water molecules [21, 22]. The presence of the C-H stretching and bending vibrations of the -CH<sub>2</sub>- group was identified by the two small bands at 2940–2850 cm<sup>-1</sup> and 1455 cm<sup>-1</sup>, respectively [23- 25]. As a result, the organic residuals which act as stabilizers controlled the aggregation of ultrafine nanoparticles, enhancing the stability of the as-obtained QDs.

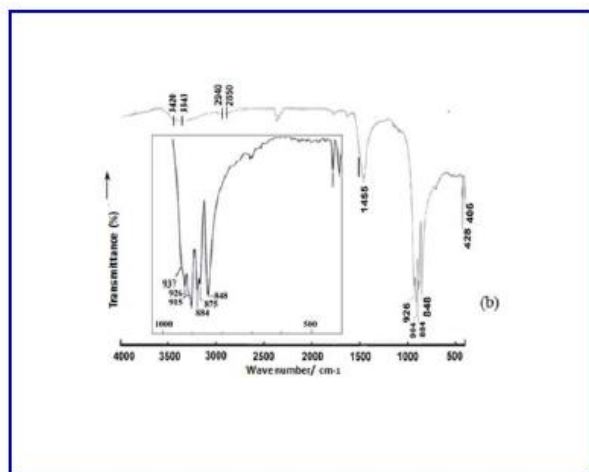


Fig.2: FT-IR spectrum of (SCO) Sample heat treated at 800°C for 4h.

The overview morphology of the sample (SCO) was observed by SEM (Fig.3). The low magnification SEM of the sample reveals the highly porous structure of the fluffy sample while the high magnification reveals the fine and hairy microstructure. The elemental identification and quantitative compositional information is further confirmed by energy dispersive x-ray (EDX) analysis. Profile in (Fig.3) represents the relative atomic abundance of O, Cr and Sr species present in the surface layers of the as prepared sample. EDX analysis supports the above results, indicating that Strontium and oxygen are the most abundant elements of the obtained surface structure. Clearly, the EDX detected value of carbon content in the sample is owing to the carbon tape used in the procedure for samples processing and / or traces of the organic ligands.

To obtain clear insight into the assembled structure of the as-prepared NPs (SCO), transmission electron microscopy (TEM) and high-resolution TEM (HR-TEM) in association with the selective area electron diffraction were performed and the corresponding images are shown in (Fig.4). In agreement with the XRD analysis above, the low-magnification TEM images (Fig. 4a) show that numerous ultrafine NPs are uniformly anchored on the SrCrO<sub>4</sub> with a bright and uniform distribution. Interestingly, magnified views of the crystalline NPs (Fig. 4b and 4c) clearly indicate that the particles are in the nanosize range (10-40 nm) whereas those of the QDs are in the range of less than 1 nm. The TEM micrograph (Fig.5c) clearly indicates the formation of three- dimensional, close packed glassy nanocrystal solid [26]. QDs NPs show arbitrary oriented

crystallites, while the bigger crystallites NPs show spherical shapes.

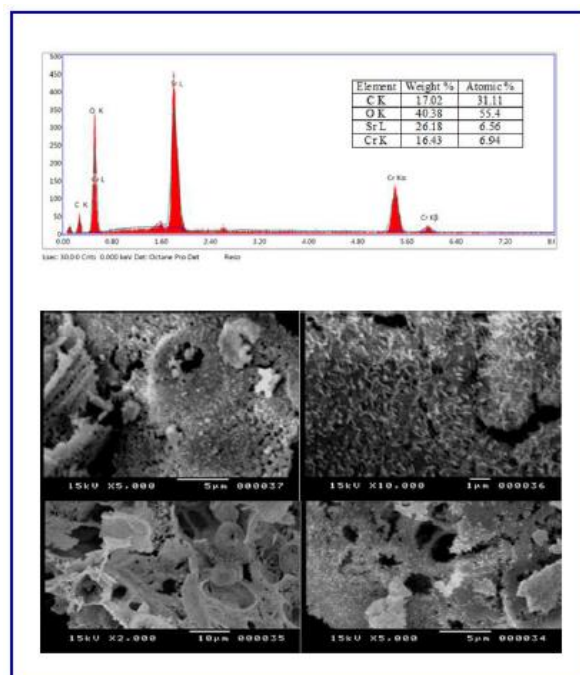


Fig.3: EDX - spectra of (SCO) phases (a) and SEM of (SCO) sample at different Magnifications.

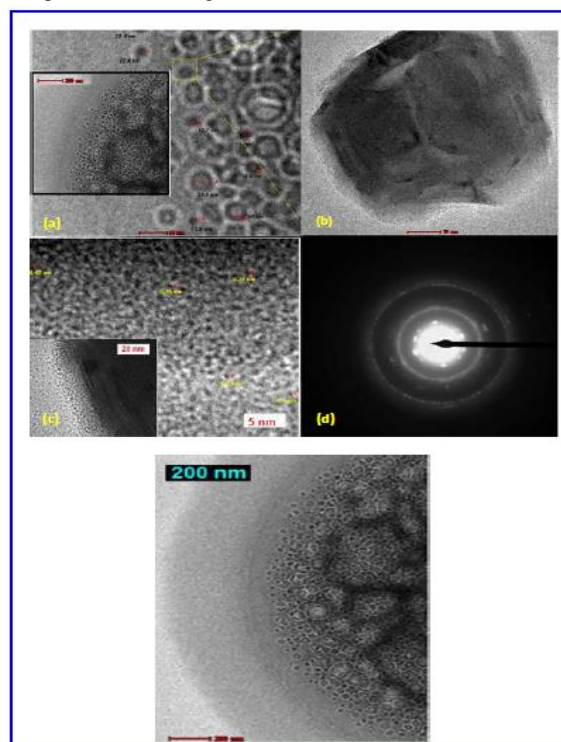


Fig.4: HRTEM micrographs (a- c) and the electron diffraction pattern (d) of (SCO) self- assembled phases.

The electron diffraction pattern (Fig. 4d) further exhibits a polycrystalline nature; indicate the presence of more than one phase. The TEM image (Fig. 5a) and XRD pattern (Fig.5b) corresponds to (SCO)\* clearly explains the effect of surfactant (CA)

concentration on morphology and particle size of Sr-Cr-O system. In our experiment, the concentration of citric acid introduced compared to the total amount of precursors was (12 and 20 % for samples (SCO) and (SCO)\*, respectively). (Fig. 5a) clearly shows that the particle size of (SCO)\* increases up to 60 nm compared to sample (SCO) (Fig. 5). Moreover, the x-ray diffraction results showed in (Fig.6c) indicate the existence of the same characteristic bands of SrCrO<sub>4</sub>, SrCrO<sub>3</sub> and SrO<sub>1.95</sub> but with different particle size and less crystallinity.

### 3.3. Electrical Conductivity

The electric conductivity of the Sr-Cr-O system calcined at 800°C samples (SCO) and (SCO)\* have been measured at room temperature and found to be  $6 \times 10^{-4}$  and  $0.18 \times 10^{-4}$  S.m<sup>-1</sup>, respectively expected to increase greatly at higher temperatures according to electric conductive behavior of semiconductors.

Since SrCrO<sub>4</sub> is p-type semiconductor whose electric conductivity is too low to support fast electron transport required by high rates, the combination of nanostructured phases with the co-existence of Cr<sup>4+</sup>-Cr<sup>6+</sup> couple pairs (SrCrO<sub>3</sub>-SrCrO<sub>4</sub>) may form the so called mobile-electron Zener phase [27, 28]. The difference in electrical conductivity between (SCO) and (SCO)\* may be attributed to the difference in particle size between the two samples as well as the co-existence of QDs embedded in SrCrO<sub>4</sub> matrix.

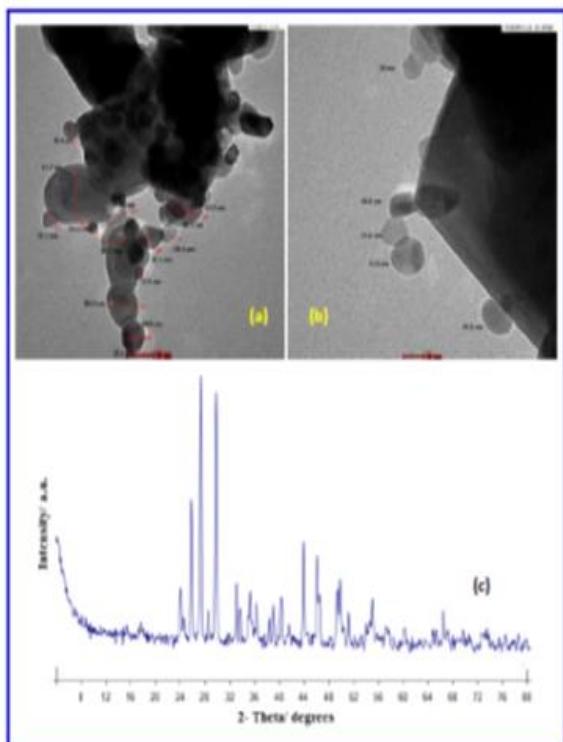


Fig5: The morphology and Structure of (SCO)\*, TEM images at different magnifications (a and b) as well as the corresponding XRD pattern (c) of (SCO)\* heat treated at 800° C for 4 h

### 3.4. Optical properties and photoactivity:

The optical properties of the as-prepared (Sr-Cr-O) semiconductor were investigated. UV- vis -DRS analysis Fig.6a, reveals the band structure of SrCrO<sub>4</sub> [29, 30] as well as the bands in the blue shift region characteristic for the presence of a narrow quantum-size distribution of nanoparticles. The optical absorption at 280 and 370 nm represent the oxygen→Cr+4 and oxygen→Cr+6 charge transfer transitions characteristic for SrCrO<sub>4</sub> [8]. Moreover, two bands (the first band is broad ranging from 580-790, centered at ≈ 680nm), the second at 430 nm are attributed to the Cr+4 3A<sub>2</sub>→3T<sub>1</sub> (3F) and 3A<sub>2</sub>→3T<sub>1</sub> (3P) transitions, respectively. [31, 32].

The band gap energy Fig.6a approximated using  $\lambda$  (nm) at the UV-Vis absorption edge, according to bensalem et al. [33]. The band gap value was found to be 2.25 eV is in accordance with the previous reports but at lower value [7, 8]. Surface modification of the SrCrO<sub>4</sub> with QDs expanded its UV-vis wavelength response from 510 nm to 525 nm (Fig.6a). Moreover, (Fig. 6a) illustrates sharp peaks at 323, 769, 784, 838 and 830 nm which is assigned to the excitonic features of the QDs. The presence of exciton effects reduces the overall energy gap of the compound [34, 35]. Moreover, excitonic effects are usually accomplished with layered structures which become stronger by lowering the system dimensions. The SEM and TEM analysis, Figures 3 and 4, support this results revealing that QDs NPs show randomly oriented crystallites, while the larger crystallites NPs exhibit spherical shapes and smooth edges that surrounded by layers of QDs.

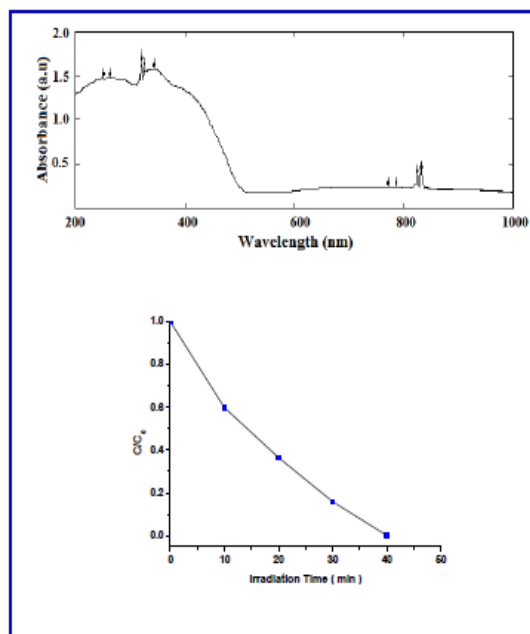


Fig.6: DRS spectrum of the photocatalyst (a) and photodegradation rate of the MB solution (C/C<sub>0</sub>) as a function of visible light irradiation time in the presence of photocatalyst (b)

The photoactivity of the self-assembled structure was evaluated by degradation of MB and the results were exhibited in Fig.6b. Under consistent irradiation conditions, the photodegradation reaction follows first-order decay kinetics. The rate constant of the catalytic reaction was seen as 0.118 min<sup>-1</sup>, with photo-degradation efficiency of 99%.

#### 4. Conclusion:

A self-assembled structure has been successfully prepared of homogenous nano-oxides composed of the (Sr-Cr-O) system via a simple approach. The solid state route of formation as well as the impacts of the QD solid self-assembly characteristics were investigated in terms of particle size and morphology. XRD and TEM studies show that the size of crystallites is about < 1 nm up to 10 nm. The optical measurement yields narrower energy band gap value and reveals that the absorption edge shifted towards the longer wavelength side. As a final conclusion this work which is interesting and under more investigations; provides a new pathway for the fabrication of ultrafine self-assembled structures of metal oxide semiconductors nanoparticles and could be used as a guide for the future design of new materials for catalysis, photocatalysis, QDs SSCs, and other applications for energy storage materials.

#### 5. Conflicts of interest:

“There are no conflicts to declare”

#### 6. References

- Zihan Wei, Serge Zhuiykov, Challenges and recent advancements of functionalization of two dimensional nanostructured molybdenum trioxide and dichalcogenides, *Nanoscale*, **11**,15709- 15738 (2019).
- Ko S. Grigoropoulos C., Hierarchical Nanostructures for Energy Devices. *The Royal Society of Chemistry*, 1- 6, (2015).
- Kongkanand A.K, Tvrdy K., Takechi M., Kuno and Kamat P.V., Quantum Dot Solar Cells Tuning Photoresponse through Size and Shape Control of CdSe-TiO<sub>2</sub> Architecture. *J.Am. Chem. Soc.*, (130) 4007–4015 (2008).
- Wang S., Kershaw S., Li G., Leung M., The self assembly synthesis of tungsten oxide quantum dots with enhanced optical properties, *J. Mater. Chem.C*, (3) 3280- 3285(2015).
- Tessier M., Mahler B., Mahler B. , Heuclin H. , Pedetti S. , B. Dubertret, Spectroscopy of Colloidal Semiconductor Core/Shell Nano platelets with High Quantum Yield, *Nano Lett.*,13 (7) 3321- 3328(2013).
- Zhang K., Sushko P., Colby R., Du Y., Bowden M. and Chambers S., Reversible nano-structuring of SrCrO<sub>3-δ</sub> through oxidation and reduction at low Temperature. *Nat. Commun.*, (5) 4669(2014).
- Yin J., Zou Z., Ye J., Photophysical and photocatalytic properties of new photocatalysts MCrO<sub>4</sub> (M= Sr, Ba), *Chem. Phys. Lett.*, (378) 24–28(2003).
- Bharat L., Reddy L., Yu J., Sol–gel synthesis, characterization and photocatalytic properties of SrCrO<sub>4</sub> particles, *Materials Letters*, (144) 85–89(2015).
- Khobragade R., Einaga H., Jain S., Saravanan G. and Labhsetwar N., Sulfur dioxide-tolerant strontium chromate for the catalytic oxidation of diesel particulate matter, *Catal. Sci.Technol.* (8) 1712-1721(2018).
- Miller R. and Tinti D., Spectroscopy chromium (VI) species, *J. Lumin.*, (36) 143 (1986).
- Smith C., A review of yellow pigments for coatings and inks, *Pigm. Resin Tech.*, (1983) 12, 15.
- Ghorai T. and Biswas N., Photodegradation of rhodamine 6G in aqueous solution via SrCrO<sub>4</sub> and TiO<sub>2</sub> nano-sphere mixed oxides, *J. Mater. Res. Technol.*, (2)10–17(2013).
- Lee S. and Huh Y., Preparation of Ultralong SrCrO<sub>4</sub> Nanowires by a Surfactant-Free Solvothermal Reaction., *Bull. Korean Chem. Soc.*, (34)1921–1923(2013).
- Chen P., Wu Q., Ding Y, Yuan P, Synthesis of SrCrO<sub>4</sub> nanostructures by onion inner-coat template and their optical properties, *Bull. Mater. Sci.*, (31), 603–608(2008).
- Wang W., Xu C., Zhen L., Yang L., Shao W., Synthesis and formation process of SrSO<sub>4</sub> sisal-like hierarchical structures at room temperature, *Cryst. Eng. Comm*, (13) 620-625 (2011).
- Standard diffraction data JCPDS files, International Center for Diffraction Data, Newton Square, PA 19073-3273, USA
- Erri P., Nader J., Varma A., Controlling Combustion Wave Propagation for Transition Metal/Alloy/Cermet Foam Synthesis, *Adv. Mater.*, (20)1243(2008).
- B. Cullity, eds., in: Elements of X-ray Diffraction, Addison-Wesley, 1978.
- Stoilova D., Georgiev M., Marinova D., Infrared Study of the Vibrational Behavior of Guest Ions Matrix-Isolated in Metal (II) Sulfates (Me = Ca, Sr, Ba, Pb), *Journal of Molecular Structure*, 738, 211–215(2005).
- Yang X., Wu Q., Lju J., 2007. Controlled synthesis of SrCrO<sub>4</sub> crystals with different morphologies *Cryst. Res. Technol.*, 42 (3) pp.211–215.

- 21- El-Sheikh S., Rabah M., Optical properties of calcium chromate 1D-nanorods synthesized at low temperature from secondary resources, *Optical Materials*, 37, 235–240 (2014).
- 22- Pereira P., de Moura A., Nogueira I., Lima M., Longo E., de Sousa Filho P., Serra O., Nassar E., Rosa I., Study of the annealing temperature effect on the structural and luminescent properties of SrWO<sub>4</sub>:Eu phosphors prepared by a non-hydrolytic sol-gel process, *J. Alloys Compd.*, 526, 11–21(2012).
- 23- Polleux J., Pinna N., Antonietti M. and Niederberger M., *J. Am. Chem. Soc.*, 127,5608-5612(2005).
- 24 -Wu S., Cao H., Yin S., Liu X. and Zhang X., Amino acid-assisted hydrothermal synthesis and photocatalysis of SnO<sub>2</sub> nanocrystals, *J. Phys. Chem. C*, 113, 17893– 17898(2009).
- 25- Zhao J., Luque R., Qi W., Lai J., Gao W., Gilaniabd M. and Xu G., The self-assembly synthesis of tungsten oxide quantum dots with enhanced optical properties, *J. Mater. Chem. A*, 3, 519–524(2015).
- 26- Chistyakov A., Zvaigzne M., Nikitenko V., Tameev A., Martynov I. and Prezhdo O., Optoelectronic Properties of Semiconductor Quantum Dot Solids for Photovoltaic Applications, *J. Phys. Chem. Lett.*, 8, 4129–4139(2017).
- 27- Zener C., 1951. Interaction between the d-Shell in the Transition Metals. II. Ferromagnetic Compounds of Manganese with Perovskite Structure, *Phys. Rev.*, 82, pp.403.
- 28- Wang, R., Wu, J. In Metal Oxides in Supercapacitors., chapter 5, Elsevier, 2017.
- 29- Tvrđy K., Frantsuzov P., Kamat P., Photoinduced Electron Transfer from Semiconductor Quantum Dots to Metal Oxide nanoparticles. *Proc Natl Acad Sci U S A.*, 108 (1), 9–34(2011).
- 30- Yang J., Ling T., Wu W., Liu H., Gao M., Ling C., Li L. and Du X., A top-down strategy towards monodisperse colloidal lead sulphide quantum dots. *Nat Commun.*, 4, 1695(2013).
- 31- Belyi M., Nedel'ko S., Chukova O., Luminescent properties of chromates of alkali metals *J. Appl. Spectrosc.* 62, 604–611(1995).
- 32- Chen P., Wu Q., Ding Y., Yuan P., Synthesis of SrCrO<sub>4</sub> nanostructures by onion inner-coat template and their optical properties. *Bull. Mater. Sci.*, 31, 603–608(2008).
- 33- Bensalem A., Bozon-Verduraz F., Delamar M., Bugli G., Preparation and characterization of highly dispersed silica-supported ceria, *Applied Catalysis A: General*, Volume 121(1) 81- 93(1995).
- 34- Mora-Sero I. and Bisquert J., Breakthroughs in the development of semiconductor- Sensitized solar cells, *J. Phys. Chem. Lett.*, (1)3046–3052(2010).
- 35- Yan K. Y., Zhang L. X., Qiu J. H., Qiu Y. C., Zhu Z. L., Wang J. N. and Yang S. H., A, Quasi-Quantum Well Sensitized Solar Cell with Accelerated Charge Separation and Collection, *J. Am. Chem. Soc.*, 135, 9531–9539(2013).

### الملخص العربي

#### تأثيرات الفيزيوكيميائية للتشكل والتجميع الذاتي للنقاط الكمومية الصلبة على أشباه الموصلات في نظام (Sr-Cr-O)

في هذه الورقة البحثية تم تشكيل المركب النانومتري الذاتي التشكل المكون من ( الكروم – الأسترنشوم- الأكسجين). الأكسيد المتكون تم تحضيره في صورة شبكة بلورية كبيرة محاطة بالنقاط الكمومية. التركيب المتكون تم التعرف عليه باستخدام تقنيات التحليل الحراري الوزني و التفاضلي، حيود الأشعة السينية ( XRD )، مطيافيه امتصاص الأشعة دون الحمراء (FT-IR)، مجهرية الإلكترون الماسح (SEM) والنافذ مطيافيه الانعكاس المنتشر للأشعة فوق البنفسجية والمرئية. التركيب النانوي الناتج وجد انه يتكون من المركب كرومات الأسترنشيم SrCrO<sub>4</sub> كصنف سائد وكل من كرومات الأسترنشيم SrCrO<sub>3</sub> و SrO<sub>1.95</sub> كصنفان ثانويان. كما اظهرت التحاليل الضوئية وجود علامات الأجزيتونات الداله على حدوث وجود الحبس الكمومي. طريقه التحضير تتضمن طريقه الترسيب. كذلك ثبتت فاعلية هذا المتراكب في الحفز الضوئي حيث تم اختباره واثبت كفاءة عالية في تكسير صبغه الميثيلين الزرقاء.